

3D-vortex labyrinths in the near field of solid-state microchip laser.

A.Yu.Okulov*

*P.N.Lebedev Physical Institute of Russian Academy of Sciences
Leninsky prospect 53, 119991 Moscow, Russia*

(Dated: January 15, 2007)

The usage of vortex labyrinths fields and Talbot lattices as optical dipole traps for neutral atoms is considered for the wavelength of trapping radiation in the range $0.98 \div 2.79 \mu m$. The square vortex lattices generated in high Fresnel number solid-state microchip lasers are studied as a possible realization. The distribution of light field is obtained via dynamical model based on Maxwell-Bloch equations for class-B laser, discrete Fox-Lee map with relaxation of inversion and static model based on superposition of copropagating Gaussian beams. The spatial patterns observed experimentally and obtained numerically are interpreted as nonlinear superposition of vortices with helicoidal phase dislocations. Such patterns are approximated analytically by a sum of array of vortex lines and additional parabolic subtrap. The separable optical trapping potential is proposed. The factorization of macroscopic wavefunction have led to analytical solution of Gross-Pitaevski equation for ensemble of quantum particles trapped in vortex labyrinth formed by spatially - periodic array of Laguerre-Gaussian beams.

PACS numbers: 03.75.Lm., 42.50.Vk., 42.60.Jf, 42.65.Sf.,47.32.Cc

I. INTRODUCTION

Optical dipole traps for neutral atoms [1] are a subject of considerable interest. A certain amount of proposals of increasing complexity of trapping EM-field appeared recently. Apart from a relatively simple geometrical patterns like standing plane-wave gratings[2], evanescent wave mirrors[3], toroidal traps which utilize the intensity distribution of Laguerre-Gaussian (LG) beams in beam waist [4] a several proposals were made which utilize the arrays of Gaussian beams, both phase-locked [5, 6] and unlocked ones [7]. The interference inherent to phase-locking provides multiply connected configurations of intensity distribution, phase gradients and electromagnetic (EM) momentum density [8, 9]. The winding EM momentum distribution is the cause of the angular momentum transfer to macroscopic bodies (e.g. dielectric ball) [10] and to trapped BEC as well [11].

The EM field configuration under consideration is based upon properties of self-imaging optical fields[12, 13]. The difference between phase-locked array of zero-order Gaussian beams and phase-locked array of optical vortices (OV) obtained experimentally in the near field of solid-state microchip laser [14] is that the latter consists of array of parallel vortex lines with opposite circulations and topological charges ℓ_{EM} (TC) (fig. 1) [5]. In contrast to earlier proposals where individual loading and addressing of trapping sites was considered [7] this OV array have sophisticated configuration of intensity [5] and EM momentum density of trapping field. Due to this configuration the BEC trapped in EM field might have macroscopic wavefunction of complex form composed of array of superfluid vortices (SFV). The cause of SFV formation is light-induced torque experienced by isolated resonant atom which interacts with Laguerre-Gaussian beam having phase singularity. It was show by Allen et al.[8] the value of torque in saturation limit is $T = \hbar \ell_{EM} \Gamma$. The origin of torque is due to nonzero azimuthal EM momentum component. The azimuthal Doppler shift corresponding to such motion had been observed[9]. This torque might have an appreciable value even in nonresonant case, although it is significantly reduced by the multiple of $(\Delta/\Gamma)^2$, where Δ - is detuning, Γ - is linewidth[8]. As a result an azimuthal component of EM momentum is transferred to atom in such a way that it will move around phase singularity - the direction of rotation is fixed by TC of trapping beam. This is the cause of circular motion of BEC confined in isolated toroidal trap.

In current paper the maximally transparent and simple analytical description presented which describes the transfer of angular momentum from optical vortex array (OVA) to trapped BEC. As a first step in *section 2* the distribution of light intensity and phase in the near field of solid-state microchip laser are computed. The configuration of intensity and phase of EM-field of OVA has complicated, multinode structure. In *sections 3* and *section 4* the spatially periodic arrays of Gaussian and Laguerre-Gaussian beams of the first order are compared. Next in *section 5* in order to get analytic solution for macroscopic wavefunction Ψ trapped by optical vortex array, the special optical pancake-like

*Electronic address: okulov@sci.lebedev.ru; URL: <http://sites.lebedev.ru/okulov>

potential (fig. 1) will be constructed. In this trapping potential the separation of variables in Gross-Pitaevsky equation[2] becomes possible. Next the procedure applied previously to elongated *sech*²- profile optical trap [15] will be used. Due to special adjustment of potential it is possible to capture an analytic approximation for Ψ in the form of superposition of elementary equispaced vortices. The topological charges and angular momenta of adjacent vortices are counter-directed in contrast to "rotating bucket" trap where angular momenta of SFV in bucket are co-directed [16, 17]. The numerical modeling via split-step FFT technique will be performed to check this approximate formula. The obtained spatial distribution of Ψ modulus and argument will be used for analysis of classical field of velocities of a trapped atom. The complex form of constructed macroscopic wavefunction Ψ trapped by optical vortex array might be interesting from the point view of diminishing the decoherence induced by environment in topological quantum computing[18].

II. SQUARE VORTEX LATTICES

Recent advances in controlling the dynamics of solid-state microchip lasers [14] offer the possibility of reliable control of spatiotemporal optical patterns. Compared to semiconductor lasers the host medium composed of dielectric crystal doped by neodymium Nd^{+3} or other rare earth ions ($Er^{+3}, Tm^{+3}, Ho^{+3}, Yb^{+3}$) have smaller gain and smaller self-phase modulation. Because of smaller nonresonant losses the heating of host crystal by radiation is not dramatic. The changes of the geometry and birefringence of host crystals, curvature and reflectivity of output couplers and spatial distribution of optical pumping give efficient control over mode structure. The square vortex lattices (SVL) observed in quasi plane parallel cavity[14] are of special interest. These lattices demonstrate high degree of spatial coherence : the relaxation oscillations of class-B high Fresnel number solid-state microchip laser [14] with Fresnel number in the range $N_f \approx 100 \div 1000$ are characterized by single peak at frequency about $(\sqrt{T_1 \tau_c})^{-1}$ ($0.3 \div 1.2 MHz$). This is the firm evidence of single-longitudinal and single transverse mode behaviour. The former theoretical analysis was based on parabolic equation, resulted from adiabatic elimination of polarization from standard set of Maxwell-Bloch equations [19]:

$$\frac{\partial E(\vec{r}, t)}{\partial t} + \frac{E(\vec{r}, t)}{\tau_c} + \frac{i c}{2k} \Delta_{\perp} E(\vec{r}, t) = \frac{\sigma c N_0 L_a E(\vec{r}, t) (1 + i \delta \omega T_2)}{2 L_r (1 + \sigma T_1 c \epsilon_0 |E|^2 / \hbar \omega)} \quad (1)$$

where τ_c - is photon lifetime in cavity, $k=2\pi/\lambda$ - wavenumber, σ - stimulated emission crosssection, $\delta\omega$ - detuning of lasing frequency from center of gain line, N_0 - density of inverted resonant atoms per unit volume, T_1 - inversion lifetime(longitudinal relaxation lifetime), L_a - thickness of active medium, L_r - length of resonator, c - speed of light, ϵ_0 - dielectric constant, $\Delta_{\perp}=\nabla_{\perp}^2$ [20]. When finite gain linewidth T_2^{-1} is taken into account in the framework of Swift-Hohenberg equation:

$$\begin{aligned} & \frac{\partial E(\vec{r}, t)}{\partial t} + \frac{E(\vec{r}, t)}{(\tau_c + T_2)} + \frac{i \tau_c c}{2k(\tau_c + T_2)} \Delta_{\perp} E(\vec{r}, t) - \\ & \frac{T_2^2}{\tau_c(\tau_c + T_2)^2} \left(\frac{\tau_c c}{k} \Delta_{\perp} + \delta \omega T_2 \right)^2 E(\vec{r}, t) = \frac{\sigma c N_0 L_a E(\vec{r}, t) (1 + i \delta \omega T_2)}{2 L_r (1 + \sigma T_1 c \epsilon_0 |E|^2 / \hbar \omega)} \end{aligned} \quad (2)$$

, the square vortex lattices were obtained numerically[21]. The additional term with the square of transverse laplacian is responsible for transverse mode selection due to finite gain linewidth. An alternative model with discrete time step equal to $\tau = 2L_r/c$ (time of bouncing of radiation between mirrors) utilizes the standard rate equations of class-B laser written at n -th step for electric field[5, 22]:

$$E_{n+1}(\vec{r}) = f(E_n(\vec{r})) = \frac{\sigma L_a N_n(\vec{r}) E_n(\vec{r}) (1 + i \delta \omega T_2)}{2} + E_n(\vec{r}), \quad (3)$$

inversion:

$$N_{n+1}(\vec{r}) = N_n(\vec{r}) + \left[\frac{N_0(\vec{r}) - N_n(\vec{r})}{T_1} - \sigma N_n(\vec{r}) c \epsilon_0 |E_n|^2 / \hbar \omega \right] \frac{2L_r}{c}, \quad (4)$$

and nonlocal integral mapping evaluating the field via fast Fourier transform at each timestep:

$$E_{n+1}(\vec{r}) = \int_{-\infty}^{\infty} \int_{-\infty}^{\infty} K(\vec{r} - \vec{r}') f(E_n(\vec{r}')) d^2 r', \quad (5)$$

The kernel K for the nearly plane-parallel Fabry-Perot cavity of microchip laser with transverse filtering via aperture $D(\vec{r}')$ has the form [12] :

$$K(\vec{r} - \vec{r}') = \frac{ikD(\vec{r}')}{2\pi L_r} \exp [ik(\vec{r} - \vec{r}')^2/2L_r]. \quad (6)$$

The following parameters were chosen in numerical simulation: $T_1 = 2 \cdot 10^{-4} \text{sec}$, $L_r = 1 \text{mm}$, for Nd^{+3} -doped crystals $\sigma = (1.2 - 0.6) \cdot 10^{-20} \text{cm}^2$, $N_0 = 10^{16} \text{cm}^{-3}$, $\delta\omega T_2 = 0.1$. In numerical evaluation of eq. (5) via split-step FFT method [23] the mesh size in X, Y plane was $512 \cdot 512$ points. The "guard bands ratio" [26] was set equal to 8. The main part of the field Ψ was located inside central part of a mesh of $64 \cdot 64$ size - the "image area". The tolerance of the energy spillover was kept within $\epsilon_1 = 0.001$. The "windowing" in wavenumber space after FFT at each timestep was performed by usage of "Fermi-Dirac" smoothed step function [23]. The dissipation inherent to "windowing" in split-step FFT method was compensated by nonlinear gain. The initial conditions for field E_n were taken as multimode random field [23].

Just near lasing threshold the radiation mode has a distribution of intensity as rectangular grating of bright and dark spots : the latter are vortex cores. The nonlocal integral mapping proved to be successful in computation of the near field distribution as well. Quite unexpectedly in the most runs the parallel vortex lines were obtained (fig. 1) [5] rather than periodic array of bright and dark spots, typical to Talbot phenomenon[12]. The origin of parallel vortex lines is interpreted as nonlinear superposition of vortices with helicoidal phase dislocations. In the next *section 3* and *section 4* the possibility of approximation of this nonlinear optical vortex lattice by linear equivalent will be outlined.

III. TALBOT LATTICES

Consider the phase-locked rectangular lattice of zero-order Gaussian beams located at sites $\vec{r}_{jx, jy}$ [12] separated by period p , where jx, jy - are discrete indices corresponding x and y coordinate of a given site. Let us assume for simplicity that polarization is linear, thus spin of light is zero. At $z = 0$ plane the electric field E is given by expression:

$$E(\vec{r}, 0) = E_0 \sum_{jx, jy} \exp [-|\vec{r} - \vec{r}_{jx, jy}|^2/(2d^2)] \quad (7)$$

After paraxial propagation of distance z the electric field $E(\vec{r}, z)$ is transformed into:

$$E(\vec{r}, z) = E_0 \frac{i \exp [ikz]}{(1 - iz/kd^2)} \sum_{jx, jy} \exp \left[-\frac{|\vec{r} - \vec{r}_{jx, jy}|^2}{2d^2(1 - iz/(kd^2))} \right] \quad (8)$$

The constructive interference between adjacent beams produces periodic interference patterns in different z -spaced planes. The initial periodical pattern is reproduced at so-called Talbot-distances $z_t = 2p^2/\lambda$. In the intermediate planes $z_t/4m$ the coarser lattices with periods p/m are produced[23, 24]. As a result a 3D lattice of bright spots is formed (fig. 2).

Each spot could serve as potential well for neutral atoms [1, 2, 5, 6], because intensity gradient will attract or repulse the atomic dipoles depending the sign of detuning of radiation frequency from resonance. At low frequencies (red-detuning) atomic dipole oscillates in-phase with trapping field and tries to align parallel to electric field. Thus potential energy of dipole $U = -\vec{p} \cdot \vec{E}(\vec{r})/2$ is lower in local maxima of intensity and atoms are collected at bright spots. On the other hand at frequencies above the resonance (blue-detuning) atomic dipole oscillates out-of-phase and it has tendency to align anti-parallel to electric field. In this blue-detuned case the potential energy of dipole is higher in local maxima of intensity and atoms are repelled into dark regions.

Such geometry of trapping in integer and fractional Talbot planes based on superposition of co-propagating zeroth-order Gaussian beams was considered earlier[5] including possibility of manipulation of optical lattice geometry via mutual polarization [6] of constituting beams.

IV. ARTIFICIAL VORTEX LABYRINTH

Consider now the periodic array of Laguerre-Gaussian vortex beams with helicoidal phase dislocations (fig. 3):

$$E(\vec{r}, z = 0) \approx E_0 \sum_{jx, jy} (|\vec{r} - \vec{r}_{jx, jy}|) \exp (-|\vec{r} - \vec{r}_{jx, jy}|^2/d^2) \exp (-|\vec{r}|^2/D^2) \exp [i \ell_{EM} \text{Arg}(\vec{r} - \vec{r}_{jx, jy}) + i \pi(jx + jy)]. \quad (9)$$

The topological charge ℓ_{EM} is assumed to be unity, the neighbouring beams (components of the sum (9)) are π -shifted. The apodization function $exp(-|\vec{r}|^2/D^2)$ is added in order to suppress the maximum of interference pattern at the edge of array. The beams centers are placed in the centers of rectangular grid $\vec{r}_{jx,jy}$ of period p whose axes are parallel to X,Y . The overlapping beams produce interference pattern formed by two arrays of bright and dark spots rotated at 45° angle with respect to initial array of LG beams. The dark spots are of two kinds: one lattice of spots coincides with lattice of initial vortices(9), the other one is produced by interference and it is shifted at distance $p/\sqrt{2}$ along diagonal of initial lattice. The resulting interferogram has apparent 45° tilt compared to lattice of initial vortices (fig. 3).

The topological charges of dark spots (vortices) flip from one site to another. The interesting feature of this interference pattern is the distribution of angular momentum [13]. The initial array of LG beams carries unit circulation and corresponding angular momentum at each site. Such *chessboard-like* interferogram (fig. 3) contains additional array of vortices with alternative charges. The net angular momentum tends to be close to zero, because at the central part of array each positively directed TC ℓ_{EM} is compensated by four adjacent negative ones having charge $-\ell_{EM}$. The elementary cell of such a lattice consists of two π -shifted initial vortices with co-directed charges ℓ_{EM} located at diagonal and two counter-directed charges $-\ell_{EM}$ (π -shifted too) placed at the other diagonal of cell. The period p of initial pattern in numerical recipes [5] was taken as $30\mu m$ while width of each initial beam was set $w_{LG} = 22\mu m$ in order to provide significant mutual overlapping of vortices.

The longitudinal distribution of intensity of optical vortex array is composed of periodically spaced (with period p) hollow tubes - vortex cores (fig. 3). Apart from Talbot gratings which are reproduced by diffraction at $z_t = 2p^2/\lambda$ planes with corresponding period division in between planes the vortex array under consideration keeps its shape within Rayleigh range, i.e. at distances $z < D^2/\lambda$. Within this distance the diameter of cores is kept constant along z by virtue of interference of adjacent vortices, whose helical wavefronts are perfectly matched within elementary cell (fig. 4).

Consider now the interaction of individual atoms with single optical beam carrying topological charge. The gradient force will attract the "red"-detuned atomic dipole to the intensity maximum of an isolated first order Laguerre-Gaussian beam - "doughnut" beam (fig. 4), i.e. to the ring-shaped area around phase singularity. As a result the cloud of cold atoms will be accumulated near the maximum of intensity or "doughnut" as follows from variational solution of Gross-Pitaevsky equation (GPE) [2]:

$$i\hbar \frac{\partial \Psi(\vec{r}, t)}{\partial t} = -\frac{\hbar^2}{2m} \Delta \Psi(\vec{r}, t) + V_{ext}(\vec{r}) \Psi(\vec{r}, t) + \frac{4\pi\hbar^2 a}{m} \Psi(\vec{r}, t) |\Psi(\vec{r}, t)|^2, \quad (10)$$

with trapping potential V_{ext} of the form

$$V_{ext}(\vec{r}) = \frac{m\omega_z^2 z^2}{2} - Re[\alpha(\omega)] |E_0|^2 [r^2 exp(-r^2/(2w_{LG}^2))] \quad (11)$$

where $\alpha(\omega)$ is polarizability of atom[1], m - mass of particle, a - scattering length.

The approximate variational solution of GPE for ground state macroscopic wavefunction is Laguerre-Gaussian function [11]:

$$\Psi(\vec{r}, t) = |\vec{r}| exp(-|\vec{r}|^2/(2w_r^2) - z^2/(2w_z^2) + i\ell_{BEC} \phi), \quad (12)$$

where ℓ_{BEC} is the topological charge of this vortex Ψ solution. Hence the probability distribution $|\Psi(\vec{r}, t)|^2$ of finding atom some near the point $\vec{r} = (x, y, z)$ at the moment t is similar to the intensity distribution of trapping field as pointed out in [11]. More information could be obtained from the study of phase structure of wavefunction and comparison of topological charges of trapping field and BEC vortex. It is easy to realize using Madelung transform

$$\Psi(\vec{r}, t) = \sqrt{\rho(|\vec{r}|, \phi, t)} exp(i\theta(|\vec{r}|, \phi, t)) \quad (13)$$

that there exists flow of "probability fluid" with velocity \vec{v} proportional (parallel) to the phase gradient lines:

$$v(\vec{r}, t) = \frac{\hbar}{m} \nabla \theta(\vec{r}, t) \quad (14)$$

Such "flow of wavefunction" occurs around the z -axis (beam axis). The "flow" described by (12) is potential and conservative as it should be for superfluid. This picture is complicated by vorticity of EM-momentum, inherent to

LG-beams [9]. Strictly speaking the rotation of classical dipole around core is accelerated by nonconservative torque induced by azimuthal force circulating around vortex core. For two-level atom the value of torque T is given by following expression obtained by Babiker, Power and Allen [8]:

$$T = \hbar \ell_{EM} \Gamma \left[\frac{I_L}{1 + I_L + \Delta^2/\Gamma^2} \right] \quad (15)$$

where I_L - normalized trapping field intensity, $\Delta = \omega - \omega_0$ - detuning of trapping field frequency ω from resonant frequency ω_0 of dipole. In saturation limit T is simply : $T = \hbar \ell_{EM} \Gamma$. In nonresonant case this torque reduces as Γ^2/Δ^2 . At trapping frequencies of Nd^{+3} laser $\Delta = 10^{14}Hz$ and $GaAs$ laser $\Delta = 10^{13}Hz$ the D -line doublet of ^{85}Rb with linewidth $\Gamma = 5 \cdot 10^6 Hz$ [1] the torque is reduced by factor depending on laser intensity I_L . Thus due to trade-off between the saturation and detuning the torque exists both near and at large detuning from the resonance. Consequently the loop integral of the azimuthal force over circular trajectory around core $\oint (\vec{F}_t \times \vec{r}) \cdot d\vec{l}$ is nonzero (fig. 4).

In classical picture because of this torque the dipole placed in the doughnut beam will move "upwards" the helicoidal phase staircase, i.e. it will rotate around LG-beam axis. The direction of rotation is determined by topological charge ℓ_{EM} of the trapping beam (fig. 4). Qualitatively classical dipole is pushed by azimuthally periodic electric field - it happens because the phase of electric field oscillations at each point in circle around the center of beam is shifted with respect to neighbouring points. Thus classical dipole placed at maximum of intensity of GL-beam will feel the "plane-wave-like" nonresonant pressure of light field. The associated azimuthal Doppler shift of the moving atom was observed experimentally recently [25]. Outside the resonance the origin of torque T is interpreted in similar way: the Poynting vector has component $S(\vec{r})_t$ tangent to helix and local flux of electromagnetic momentum pushes dipole along phase gradient, i.e. in azimuthal direction. The local density of EM-momentum $\vec{g} = \vec{S}/c^2$ is proportional to components of Poynting vector[9]:

$$\begin{aligned} S(\vec{r})_t &= \frac{\epsilon_0 \omega \ell_{EM} c^2}{r} |E(\vec{r})|^2 \\ S(\vec{r})_z &= \epsilon_0 c |E(\vec{r})|^2, \end{aligned} \quad (16)$$

where $S(\vec{r})_t$ - is tangential component of Poynting vector, $S(\vec{r})_z$ - is axial one, $|\vec{r}|$ - is the distance from optical vortex core, ω - is frequency of trapping field. The existence of tangential component of Poynting vector became visible when macroscopic dielectric ball with radius larger than LG-beam core and comparable to "doughnut" radius is placed in center of LG-beam. The rotation of particle is induced via such torque and corresponding transfer of the angular momentum[10].

When loaded in optical vortex lattice (fig. 5) the atomic dipole will move around the adjacent vortex core with acceleration. The radius of rotation will increase until the dipole will approach the separatrix of the velocity fields. Next after certain amount of rotations around the vortex core it could jump to another vortex using bright areas between vortices as bridge (fig. 4). This qualitative picture is complicated by azimuthally inhomogeneous distribution of intensity around each core.

Our aim now is to show that just described classical motion have quantum mechanical counterpart. The transfer of angular momentum results in the specific form of macroscopic wavefunction Ψ maintaining coherence all over trapping array:

$$\begin{aligned} \Psi(\vec{r}) &\approx \sum_{jx,jy} (|\vec{r} - \vec{r}_{jx,jy}|) \exp(-|\vec{r} - \vec{r}_{jx,jy}|^2/d^2) \\ &\exp(-|\vec{r}|^2/D^2) \exp[i \ell_{BEC} \text{Arg}(\vec{r} - \vec{r}_{jx,jy}) + i \pi(jx + jy)]. \end{aligned} \quad (17)$$

Next section presents the method of solution of Gross-Pitaevsky equation with vortex trapping field $E(\vec{r})$ in the form (9).

V. SEPARABLE VORTEX ARRAY POTENTIAL FOR BEC

In order to get closed form solution for macroscopic Ψ it is worth to mention that azimuthal accelerating force has very small value, falling as Δ^{-2} under detuning from resonance[8]. Next let us introduce optical potential V_{ext} as a square modulus of trapping field $E(r_{\perp}^2, z)$ [1]. The torque T will be taken into account as a "selection" rule for choosing distribution of topological charges ℓ_{BEC} in resulting solution.

It was shown recently [15] that Gross-Pitaevsky equation[2] in 3D-configuration:

$$i\hbar \frac{\partial \Psi(\vec{r}, t)}{\partial t} = -\frac{\hbar^2}{2m} \Delta \Psi(\vec{r}, t) + V_{ext}(\vec{r}) \Psi(\vec{r}, t) + \frac{4\pi\hbar^2 a(\vec{B})}{m} \Psi(\vec{r}, t) |\Psi(\vec{r}, t)|^2, \quad (18)$$

admits the application of standard method of separation of variables widely used for solution of *linear* partial differential equation, e.g. in quantum mechanics. The separation of variables means that wavefunction is factorized:

$$\Psi(\vec{r}, t) = \Psi_{\perp}(\vec{r}_{\perp}, t) \Psi_{\parallel}(z, t) \quad (19)$$

provided the Hamiltonian is the sum of two components. First component depends on a longitudinal variable z and a second component depends upon transverse variables \vec{r}_{\perp} .

Following to [15] in order to separate variables and factorize the wavefunction let us choose trapping potential in the following form, as a sum of components depending on longitudinal coordinate z and transverse coordinates \vec{r}_{\perp} separately:

$$V_{ext}(\vec{r}_{\perp}, z) = V_z + V_{\perp} = \frac{m\omega_z^2 z^2}{2} - Re[\alpha(\omega)] |E(\vec{r}_{\perp})|^2 + \frac{m\omega_{\perp}^2 |\vec{r}_{\perp}|^2}{2} \quad (20)$$

where $\alpha(\omega)$ is atomic polarizability[1] :

$$\alpha(\omega) = 6\pi\epsilon_0 c^3 \frac{\Gamma/\omega_0^2}{(\omega_0^2 - \omega^2 - i(\omega^3/\omega_0^2)\Gamma)} \quad (21)$$

The $\alpha(\omega)$ is assumed to be real due to large negative ("red") detuning from atomic resonance at frequency $\omega_0 = 2.4 \cdot 10^{15}$ Hz. The imaginary part of denominator under detuning $\Delta = \omega - \omega_0$ for ^{85}Rb atoms trapped by EM-field at $\lambda = 1.06 \div 0.808 \mu\text{m}$ is $(3 \div 4.7) \cdot 10^8$ times smaller than real part, so the permittivity of atom $\alpha(\omega)$ is real with good accuracy [1]. The trapping field $E(\vec{r}_{\perp})$ is assumed to be periodic function of transverse variables $\vec{r}_{\perp} = (x, y)$, composed of LG beams placed at the nodes (jx, jy) of rectangular grid of period p (9).

The additional parabolic well with frequency ω_{\perp} is introduced in (20) to get analytical solution for one trapping vortex. In order to avoid the interference between different trapping beams the usage of different carrier frequencies is recommended for longitudinal parabolic well $\frac{m\omega_z^2 z^2}{2}$, vortex array beam $E(\vec{r})$ and parabolic subtrap in (20). The characteristic scales of potential in longitudinal direction and transverse direction are chosen to form "pancake trap" : $\omega_z \gg \omega_{\perp}$ (fig. 1). The opposite case of elongated trap with $\omega_z \ll \omega_{\perp}$ and "solitonic" longitudinal potential $V_z \approx \text{sech}^2(z)$ was considered earlier using analogous procedure [15].

The longitudinal part of wavefunction $\Psi_{\parallel}(z, t)$ is obtained as a ground state of 1D harmonic oscillator:

$$i\hbar \frac{\partial \Psi_{\parallel}}{\partial t} = -\frac{\hbar^2}{2m} \frac{\partial^2 \Psi_{\parallel}}{\partial z^2} + \frac{m\omega_z^2 z^2}{2} \Psi_{\parallel} \quad (22)$$

$$\Psi_{\parallel} = \left(\frac{m\omega_z}{\pi\hbar}\right)^{1/4} \exp[-m\omega_z z^2/(2\hbar) - i\omega_z t] \quad (23)$$

The transverse part of wavefunction $\Psi_{\perp}(\vec{r}_{\perp}, t)$ is to be obtained by solving "transverse" GPE:

$$i\hbar \frac{\partial \Psi_{\perp}}{\partial t} = -\frac{\hbar^2}{2m} \Delta_{\perp} \Psi_{\perp} + V_{\perp}(\vec{r}_{\perp}) \Psi_{\perp} + \frac{4\pi\hbar^2 a(\vec{B})}{m} \Psi_{\perp} |\Psi_{\perp}|^2 \left[\int_{-\infty}^{\infty} |\Psi_{\parallel}(z, t)|^4 dz \right] / \left[\int_{-\infty}^{\infty} |\Psi_{\parallel}(z, t)|^2 dz \right], \quad (24)$$

where

$$V_{\perp} = \frac{m \omega_{\perp}^2 |r_{\perp}^{\vec{r}}|^2}{2} - Re[\alpha(\omega)] |E(r_{\perp}^{\vec{r}})|^2 \quad (25)$$

Because of normalization

$$\int_{-\infty}^{\infty} |\Psi_{\parallel}(z, t)|^4 dz = 1/2 \quad \text{and} \quad \int_{-\infty}^{\infty} |\Psi_{\parallel}(z, t)|^2 dz = 1 \quad (26)$$

The following 2D GPE results from separation of variables for "pancake" trap:

$$i\hbar \frac{\partial \Psi_{\perp}}{\partial t} = -\frac{\hbar^2}{2m} \Delta_{\perp} \Psi_{\perp} + V_{\perp}(r_{\perp}^{\vec{r}}) \Psi_{\perp} + \frac{2\pi\hbar^2 a(\vec{B})}{m} \Psi_{\perp} |\Psi_{\perp}|^2 \quad (27)$$

The scattering length a as a function of magnetic field is:

$$a(\vec{B}) = a_{bg} \left(1 + \frac{\Delta_B}{B - B_R}\right) \quad (28)$$

where Δ_B is a width of Feshbach resonance, B_R - resonant magnetic field, a_{bg} -background scattering length[2].

Formally the separation of variables is applicable each time when Hamiltonian is a sum of components depending on different groups of variables, but this method have additional physical meaning for asymmetric potentials. The examples are elongated in z -direction trap [15] and "pancake" 2D trap (fig. 1) as in current case. The dynamics of Ψ in 2D traps was considered in large amount of papers, including the geometries of periodic potentials, Bessel lattices etc. In current case the SFV lattice under consideration has some features, qualitatively described above in discussion of classical motion of dipole around phase singularity.

The continuous transfer of angular momentum from optical vortex to BEC with wavefunction Ψ might induce the vortices in initially nonrotating BEC. Because the direction of rotation of classical particle is determined by distribution of TC of optical vortices ℓ_{EM} of trapping beam the distribution of TC's in quantum superfluid lattice ℓ_{BEC} will be set identical to those of trapping field.

The possible solution of equation (27) presumes the identical spatial distributions for fields $\Psi_{\perp}(r_{\perp}^{\vec{r}}, t)$ and $E(r_{\perp}^{\vec{r}})$. It means that Ψ is also a sum of a LG functions with alternating topological charges ℓ_{BEC} (see eq.(17)). Unfortunately the effective diameter of the core b is much larger than effective size of LG beam bottleneck (4-10 μm). But this discrepancy does affect the basic features of solution because of logarithmic dependence of vortex energy on vortex dimensions [17].

The correlation K of two complex spatially inhomogeneous fields $\Psi_{\perp}(r_{\perp}^{\vec{r}}, t)$ and $E(r_{\perp}^{\vec{r}})$ is expected to be unit:

$$K = \frac{|\int \Psi_{\perp} E^*(r_{\perp}^{\vec{r}}) d^2 r_{\perp}^{\vec{r}}|^2}{[\int |\Psi_{\perp}|^2 d^2 r_{\perp}^{\vec{r}}][\int |E(r_{\perp}^{\vec{r}})|^2 d^2 r_{\perp}^{\vec{r}}]} = 1 \quad (29)$$

The key point is in adjusting the parameters in $\Psi_{\perp}(r_{\perp}^{\vec{r}}, t)$ and $E(r_{\perp}^{\vec{r}})$ in such a way that two last terms in (24) would cancel each other. This might happen when following condition is imposed upon the coefficients:

$$Re[\alpha(\omega)] |E_0|^2 = \frac{2\pi\hbar^2 a(\vec{B})}{m} \quad (30)$$

The mutual compensation of these two terms could be achieved via tuning of magnetic field \vec{B} near Feshbach resonance.

Consider first the case of single vortex trap collocated with a single parabolic subtrap:

$$V_{\perp} = \frac{m \omega_{\perp}^2 r^2}{2} - Re[\alpha(\omega)] |E_0|^2 r^2 \exp[-r^2/d^2] \quad (31)$$

The following exact solution for 2D harmonic oscillator is known :

$$\Psi_{\perp} = \sqrt{\frac{2}{\pi}} \left[\frac{m\omega_{\perp}}{\hbar}\right]^{3/2} r \exp\left[-\frac{m\omega_{\perp}^2 r^2}{2\hbar} + i\phi \ell_{BEC} - i2\omega_{\perp} t\right] \quad (32)$$

which is similar to variational solution for "transverse" wavefunction (12) [11]. Note in our case the exact wavefunction of the transversal GPE found, rather than variational one (12). The stability analysis will be published elsewhere. The angular momentum per particle is given by:

$$\langle \hat{\ell} \rangle = \int \int \Psi_{\perp}^* (-i\hbar) \frac{\partial \Psi_{\perp}}{\partial \phi} d^2 r_{\perp} = \hbar \quad (33)$$

where ϕ is azimuthal angle (fig. ??). Again SFV carries angular momentum \hbar per particle and kinetic energy of the whole vortex line $E_{kin} = \rho \pi \hbar^2 \chi \ln(\tilde{b}/\tilde{a})/m$ [17]. Consider now the trapping of BEC by of phase-locked Gaussian-Laguerre beams placed at the nodes i, j of rectangular grid of period p (see Eq. 9).

Let us assume for simplicity that optical wavelength λ is equal to De-Broigle wavelength λ_{db} :

$$\lambda = \lambda_{db} = \frac{\hbar}{\sqrt{2mk_B T}} \quad (34)$$

The corresponding BEC temperature for ^{85}Rb atoms is:

$$T = 1.7^{-7} K \quad (35)$$

After imposing compensation condition (26) the residual part of transverse GPE (27) corresponds to free-space evolution:

$$i\hbar \frac{\partial \Psi_{\perp}}{\partial t} = -\frac{\hbar^2}{2m} \Delta_{\perp} \Psi_{\perp} + \frac{m \omega_{\perp}^2 r^2}{2} \Psi_{\perp} \quad (36)$$

The free space propagation (fig. 1) equation for EM-field will be of similar form:

$$\frac{\partial E}{\partial z} = -\frac{i}{2k} \Delta_{\perp} E + \frac{k r^2}{2f_{cavity}} E \quad (37)$$

where f_{cavity} is effective focal length of the laser cavity (fig. 1) induced by thermal lens collocated with inhomogeneity of optical pumping.

Because of linearity of equation and superposition principle the solution of (37) will be the sum of free-space modes including zero-order Gaussian functions, Gaussian-Hermit or Laguerre-Gaussian modes located at sites $\vec{r}_{jx, jy}$ [12] separated by period p . The axes of such optical array are parallel to X, Y . In order to solve numerically eq. (27) the split-step FFT method [23] was used. The mesh size in X, Y plane was $512 \cdot 512$ points, the "guard bands ratio" [26] was chosen equal to 8. So the main part of the field Ψ was located inside central part of a mesh which had $64 \cdot 64$ size - the "image area". The tolerance of the energy spillover was kept within $\epsilon_1 = 0.0001$. The windowing in wavenumber space after FFT at each timestep was performed by usage of "Fermi-Dirac" smoothed step function [23]. The dissipation inherent to split-step FFT method have led to decrease of total "amount of particles" $\int \int |\Psi|^2 dx dy$ within "image area" at a speed of 10^{-3} per time step. The special initial conditions of "preselected" SFV array in the form (17) superimposed upon homogeneous background gave the spatial distribution of "transverse" wavefunction Ψ_{\perp} well correlated ($K \approx 0.7$) with the OVA array distribution - the array of phase-locked Gaussian-Laguerre wavepackets of the first order :

$$\Psi_{\perp} = \frac{2}{\pi} \left[\frac{m\omega_{\perp}}{\hbar} \right]^{3/2} \sum_{jx, jy} (|\vec{r} - \vec{r}_{jx, jy}|) \exp(-|\vec{r}|^2/D^2) \exp\left[-\frac{m\omega_{\perp}^2 |\vec{r} - \vec{r}_{jx, jy}|^2}{2\hbar}\right] + i \ell_{BEC} \text{Arg}(\vec{r} - \vec{r}_{jx, jy}) + i\pi(jx + jy) - i2\omega_{\perp} t \quad (38)$$

Thus the numerical solution for Ψ_{\perp} of GPE proved to be very close to the linear combination of Gaussian-Laguerre functions. Nevertheless this solution takes into account the interference between wavefunctions of "subvortices", because the "doughnut" radius is set to be a bit more than distance between lattice nodes. The arising interference pattern is well correlated with the interference pattern produced by Laguerre-Gaussian OVA $|E(r_{\perp})|^2$ (fig. 3) with the same geometrical parameters and wavelength λ . This solution proved to be stable with respect to small harmonic perturbations.

Each SFV carries angular momentum \hbar per particle and rotational kinetic energy $E_{kin} = \rho \pi \hbar^2 \chi \ln(\tilde{b}/\tilde{a})/m$, \tilde{b} - diameter of vortex core, \tilde{a} - interatomic distance, χ - length of vortex which is roughly equal to thickness of "pancake" [17]. The energy associated with superfluid vortices is of order $10^{-(19\div 20)}J$ or $0.1 \div 1 eV$ at density of dilute ^{85}Rb gas $\rho \approx 10^{16\div 18}cm^{-3}$. In contrast to superfluid in rotating bucket where angular momenta of vortices are co-directed [16], the BEC vortices trapped by optical vortex array are counter-directed from site to site. Consequently in the net sum of angular momenta each vortice of positive topological charge is compensated by the term with negative charge and total angular momentum tends to zero. Nevertheless the mutual subtraction of angular momenta(vectorial) of adjaicent vortices in the net sum does not mean the mutual subtraction of rotational energies, which are the positive scalars. The ground state carry substantial amount of rotational kinetic energy of condensate which contains N particles of mass m per unite volume, namely $E_{rot} = N_{vortices} \rho \pi \hbar^2 \chi \ln(\tilde{b}/\tilde{a})/m$.

VI. CONCLUSION

The optical vortex arrays emitted by solid-state microchip laser were analysed from the point of view of application to optical dipole traps. Firstly the numerical modeling of thin slice microchip Fabry-Perot solid-state laser resonator gave transverse field distributions(fig. 3) well correlated with experimentally observed previously. The longitudinal intensity distribution consists of periodically spaced array of parallel hollow tubes which slowly diverge while propagating along z -axis(fig. 3). The array of phase-locked Gaussian-Laquerre beams equispaced at the nodes of rectangular lattice proved to be a reasonable approximation for experimental and numerical results as well.

For macroscopic wavefunction Ψ of BEC trapped in such complex optical field the analytical solutions of Gross-Pitaevsky equation were found. These solutions are based upon separation of variables and mutual compensation of vortex component of external trapping field via nonlinear term of GPE. The obtained wavefunctions have perfect correlation with trapping field, including distribution of topological charges, which form "antiferromagnetic-like" lattice. Within framework of this particular model the "antiferromagnetic" lattice of BEC vortices carriers total angular momentum close to zero while net rotational kinetic energy of SFV lattice tends to be equal to the sum of rotational energies of vortices. Geometrically such BEC - cloud looks like "pancake" perpendicular to z -axis.

The field of classical velocities, i.e. the field of phase gradients, obtained via Madelung transform, forms "labyrinth" structure. It means that trapped atoms move in the "pancake" plane, i.e. $x - y$ plane. The rotation of atom around some vortex core is accelerated by EM-torque. The radius of rotation is gradually increased. When particle reaches the separatrix it comes to another vortex area. The trajectory of particle in transverse plane ($x - y$ plane) is Mobius-like: because the number of optical vortices is finite, in classical picture the particle will return to initial vortex eventually after roaming for some time inside trapping "labyrinth".

In quantum picture represented via analytic solution of GPE for one trapping vortex and numerical solution for optical vortex array the coherent macroscopic wavefunction extends all over OV trapping array with transverse spatial dimension of several hundred microns. The complex field of velocities, rotational energy and high degree of correlation of SFV wavefunction with OV trapping field promise more resistance to decoherence.

The qualitative analytic solution supports the basic feature related to trapping of macroscopic particles and to BEC trapping: the transfer of OAM from optical field to superfluid. The proposed OVA trap might be interesting from the point of view of studies of quantum-classical correspondence.

The mechanism of imposing the topological charges to BEC vortices by means of manipulating the vorticity of trapping optical array could result in demonstration of macroscopic quantum interference phenomena. Evidently there are 4 possible topologically equivalent combinations of parameters of solution (38) of OV charges ($\ell_{EM} = \pm 1$) and their relative phases ($\pm \pi$). Thus there exist 4 wavefunctions Ψ having an identical probabability $|\Psi|^2$ distribution and different orientation of SFL vortices with respect to physical axes x, y of trapping setup, characterised by ℓ_{BEC} and their relative phases. The transformation of the one Ψ into another one which have different phase structure is equivalent to 90° rotation around z - axis.

-
- [1] R.Grimm, M.Weidemuller and Yu.B.Ovchinnikov, *Adv.At.Mol.Opt.Phys.* **42**, 95 (2000).
 - [2] L. Pitaevskii and S. Stringari, *"Bose-Einstein Condensation"*,Clarendon Press, Oxford, 2003.
F. Dalfovo, S.Giorgini, S.Stringari, L.P.Pitaevskii, *Rev.Mod.Phys.* **71**, 463 (1999).
 - [3] Balykin, V.I., Letokhov, V.S., Ovchinnikov, Yu.B., and Sidorov A.I, *Phys. Rev. Lett.* **60**, 2137 (1988).
 - [4] E. M. Wright, J. Arlt and K. Dholakia, *Phys.Rev. A* **63**, 013608 (2001).
 - [5] A.Yu.Okulov, *"3D-configuration of the vortex lattices in microchip laser cavity"*,
QCMC-2004, AIP Conference Proceedings, **734**, p.366 (2004).
A.Yu.Okulov, *Bulletin Lebedev Physical Institute*, **9**, p.3, Sept. (2003).

- [6] Yu.B.Ovchinnikov, Phys.Rev, **73A**, 033404 (2006).
- [7] R.Dumke, M.Volk, T. Muther, F.B.J.Buchkremer, G. Birkl and W.Ertmer, Phys. Rev. Lett. **89**, 097903 (2002).
- [8] M. Babiker, W. L. Power, and L. Allen, Phys. Rev. Lett. **73**, 1239 (1994).
- [9] V.Garces-Chavez, D. McGloin, M. J. Padgett, W. Dultz, H. Schmitzer, and K. Dholakia, Phys. Rev. Lett. **91**, 093602 (2003).
- [10] M.J.Friese, J.Euger, H.Rubinstein-Dunlop, Phys.Rev. A **54**, 1543 (1996).
N.R. Heckenberg, M.E.J. Friese, T.A. Nieminen and H. Rubinsztein-Dunlop, "Mechanical Effects of Optical Vortices". pp 75-105 ,in M. Vasnetsov (ed), *Optical Vortices*, Nova Science Publishers (1999).
- [11] J. Tempere and J. T. Devreese, E. R. I. Abraham., Phys.Rev., **64A**, 023603 (2002).
- [12] A.Yu.Okulov, JOSA **B7**, p.1045, (1990).
- [13] J.Courtial, R.Zambrini, M.R.Dennis, M.Vasnetsov, Optics Express, **14**, p.938 (2006).
- [14] Y.F.Chen, Y.P.Lan, Phys.Rev., **64A**, 063807 (2001).
Y. F. Chen, Y. P. Lan, Phys.Rev., **65**, 013802 (2001).
- [15] R.Fidele, P.K.Shukla, S.De.Nicola, M.A.Manko, V.I.Manko, F.S.Cataliotti, JETP Lett., **80**,8, p.609-613 (2004).
- [16] J.R.Abo-Shaerr, C.Raman, J.M.Vogels and W.Ketterle, Phys. Rev. Lett. **88**, 070409 (2002). I.Danaila, Phys.Rev. A **72**, 013605 (2005).
- [17] R.P.Feynman, "Statistical mechanics", Ch.11, Reading, Massachusetts (1972).
- [18] A.Yu.Kitaev, LANL e-print quant-ph/ 9707021, <http://arxiv.org> (1997).
- [19] A.F.Suchkov, JETP **22**, 1026 (1965).
- [20] A.E.Siegman, "*Lasers*". *University Science Books, Mill Valley, California*(1986).
- [21] K.Staliunas, Phys.Rev. A **48**, 1573 (1993). K.Staliunas, C.O.Weiss, JOSA B **12**, 1142 (1995).
- [22] F. Hollinger, Chr. Jung, and H. Weber, JOSA B **7**, 1013 (1990).
- [23] A.Yu.Okulov, Opt.Comm.**99**, p.350-354 (1993). J.Mod.Opt.**38**,N.10,p.1887(1991).
- [24] A.Yu.Okulov, Optics and Spectroscopy, **77**, N6,p.985 (1994).
- [25] V. Garces-Chavez, K. Volke-Sepulveda, S. Chavez-Cerda, W. Sibbett and K. Dholakia, Phys. Rev.A **66**, 063402 (2002).
- [26] E.A.Sziklas, A.E.Siegman, Appl.Opt. **14**, 1874 (1975).

List of Figure Captions

Fig.1 Conceptual view of the near field optical trap. Upper plot: Transverse (in XOY plane) distribution of intensity in the near field of solid-state microchip laser [5]. Middle: The longitudinal scale extends to 6 Talbot lengths. Z - axis is directed along optical axis of microchip laser resonator (bottom). Additional tightly confined parabolic well keeping BEC cloud localized in z - direction is depicted via potential $V(z) \approx (z - z')^2$. Such potential is assumed to be superimposed by the other microchip laser beam with cylindrical focusing lens at slightly different wavelength of radiation from the range $0.98 \div 2.79 \mu m$, in order to avoid interference. Fresnel number has value of $N_f \approx N_{vortices}^2 = 64$.

Fig.2 Diffractive self-imaging of two-dimensional lattice of 8x8 Gaussian beams with period $p = 28 \mu m$. The longitudinal cross-section at $y = 0$ plane of intensity distribution $I(x, y, z)$ presented. The lattice is self-reproduced at Talbot distance, spatial period division occurs at quarter Talbot distances and central lobe forms outside the Rayleigh range.

Fig.3 a) Intensity distribution in transverse plane of artificial Laquerre-Gaussian vortex array. Vortices (dark holes) are at nodes of rectangular *chessboard-like* grid. Letters ℓ_{EM} denote vortices with alternating topological charges, changing sign from one site of lattice to another. b) Longitudinal section of vortex array in the near field in $x-z$ plane at $y = 0$ section. The vortex lines are parallel, the topological charges ℓ_{EM} are flipping from one vortex line to another. The wavelength $\lambda = 1 \mu m$, period p of lattice both in x and y directions is $30 \mu m$.

Fig.4 a) Helicoidal phase surface of Laquerre-Gaussian beam. Atomic dipole having "red" detuning moves along phase gradient. Trajectory is located at maximum of intensity. \vec{S}_t is the component of Pointing vector tangent to helix. The major component of \vec{S}_z is directed parallel to beam propagation, i.e. along Z-axis. b) Helicoidal phase surface of Laquerre-Gaussian beam array. The elementary cell consists of four vortices. The adjacent vortices have alternating topological charges ℓ_{EM} and alternating angular momenta. In classical picture the atomic dipole moves along phase gradient of a given vortex next it jumps to another one.

Fig.5 a) The argument of macroscopic wavefunction Ψ and corresponding field of velocities obtained via Madelung transform. The superfluid vortices form the lattice with alternating topological charges $\ell_{BEC} = \pm 1$. The elementary cell consists of four BEC vortices whose locations are identical to the vortices of trapping EM-field. Horizontal pair has the same charges ℓ_{BEC} which are π -shifted with respect to each other, the vertical pair have π -shifted $-\ell_{BEC}$ charges. The alternating charges ℓ_{BEC} make the field of velocities continuous. b) The distribution of the square modulus of macroscopic wavefunction Ψ obtained via numerical modeling. The location of adjacent counter-rotating vortices ℓ_{BEC} shown.

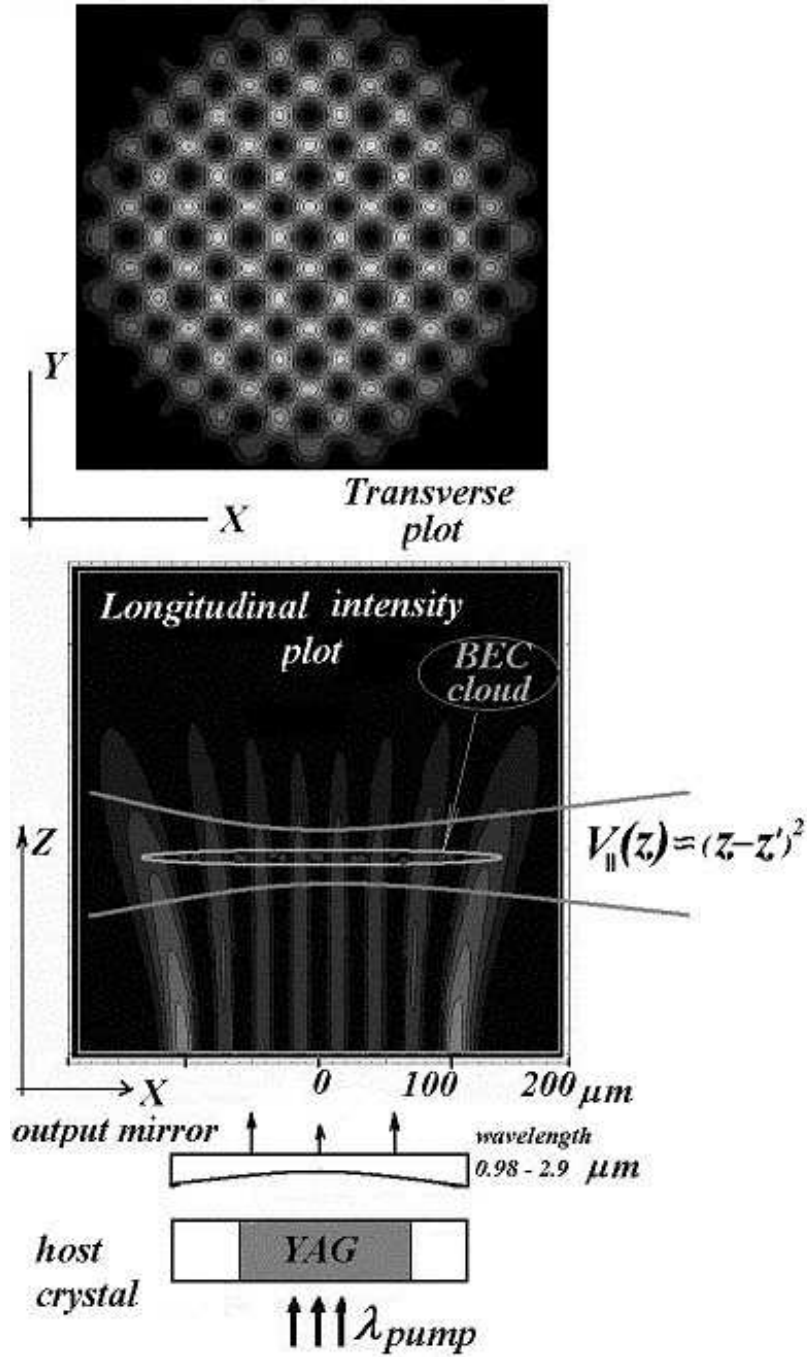


FIG. 1: Conceptual view of the near field optical trap. Upper plot: Transverse (in XOY plane) distribution of intensity in the near field of solid-state microchip laser [5]. Middle: The longitudinal scale extends to 6 Talbot lengths. Z - axis is directed along optical axis of microchip laser resonator (bottom). Additional tightly confined parabolic well keeping BEC cloud localized in z - direction is depicted via potential $V(z) \approx (z - z')^2$. Such potential is assumed to be superimposed by the other microchip laser beam with cylindrical focusing lens at slightly different wavelength of radiation from the range $0.98 \div 2.79 \mu\text{m}$, in order to avoid interference. Fresnel number has value of $N_f \approx N_{\text{vortices}}^2 = 64$.

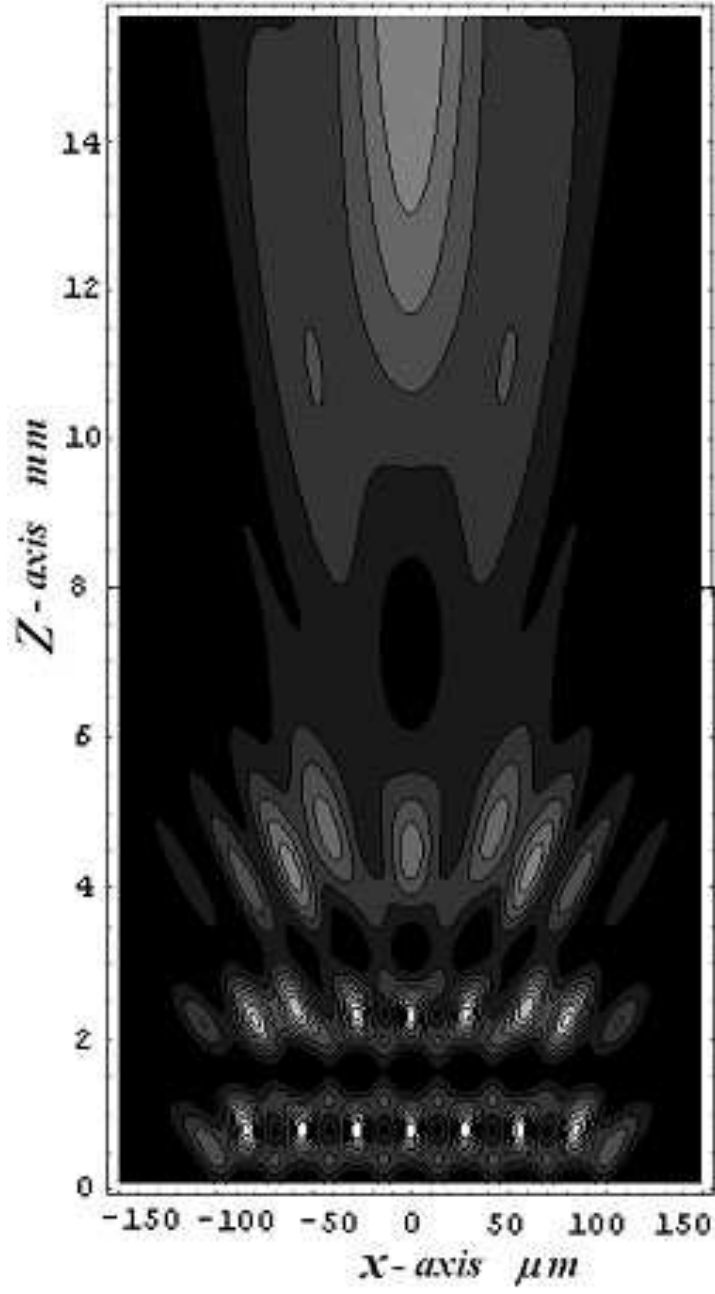


FIG. 2: Diffractive self-imaging of two-dimensional lattice of 8×8 Gaussian beams with period $p = 28 \mu m$. The longitudinal cross-section at $y = 0$ plane of intensity distribution $I(x, y, z)$ presented. The lattice is self-reproduced at Talbot distance, spatial period division occurs at quarter Talbot distances and central lobe forms outside the Rayleigh range.

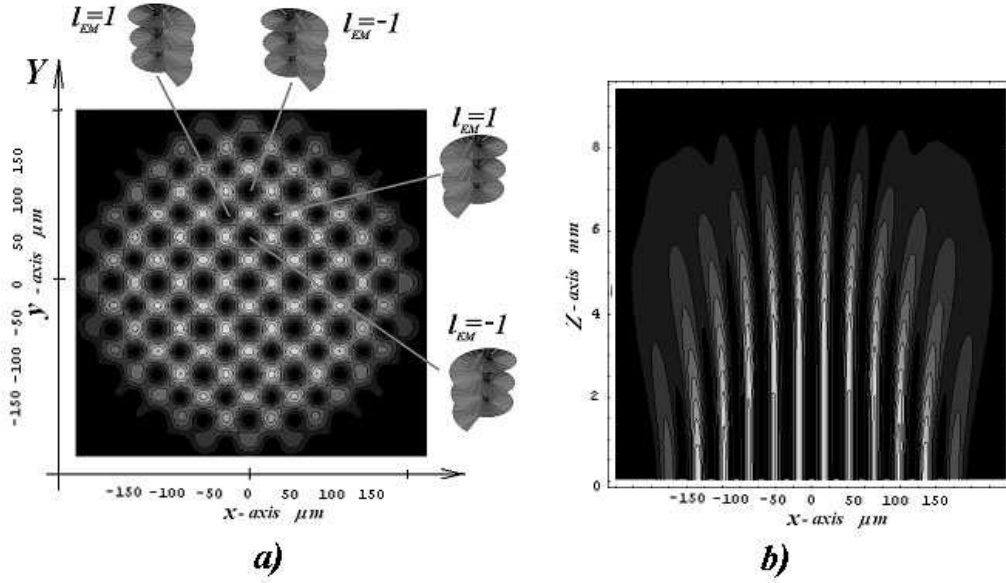


FIG. 3: a) Intensity distribution in transverse plane of artificial Laquerre-Gaussian vortex array. Vortices (dark holes) are at nodes of rectangular *chessboard* – like grid. Letters ℓ_{EM} denote vortices with alternating topological charges, changing sign from one site of lattice to another. b) Longitudinal section of vortex array in the near field in x - z plane at $y = 0$ section. The vortex lines are parallel, the topological charges ℓ_{EM} are flipping from one vortex line to another. The wavelength $\lambda = 1\mu m$, period p of lattice both in x and y directions is $30\mu m$

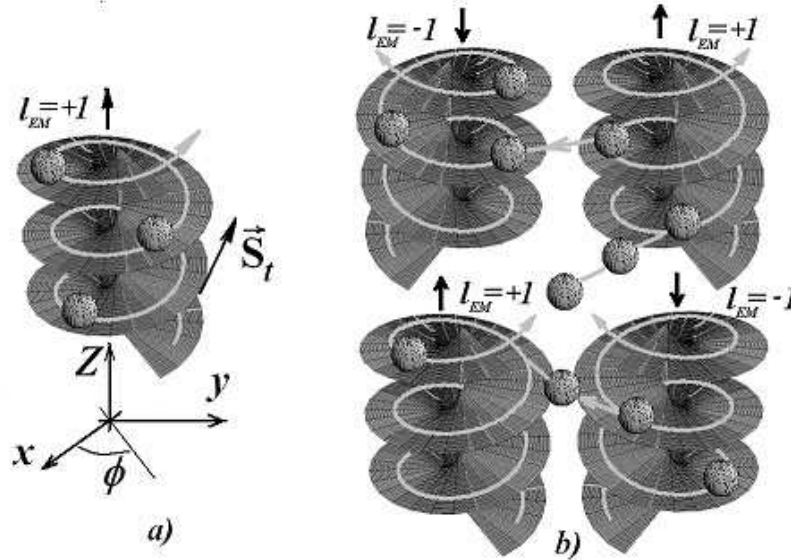


FIG. 4: a) Helicoidal phase surface of Laquerre-Gaussian beam. Atomic dipole having "red" detuning moves along phase gradient. Trajectory is located at maximum of intensity. \vec{S}_t is the component of Pointing vector tangent to helix. The major component of \vec{S}_z is directed parallel to beam propagation, i.e. along Z -axis. b) Helicoidal phase surface of Laquerre-Gaussian beam array. The elementary cell consists of four vortices. The adjacent vortices have alternating topological charges ℓ_{EM} and alternating angular momenta. In classical picture the atomic dipole moves along phase gradient of a given vortex next it jumps to another one.

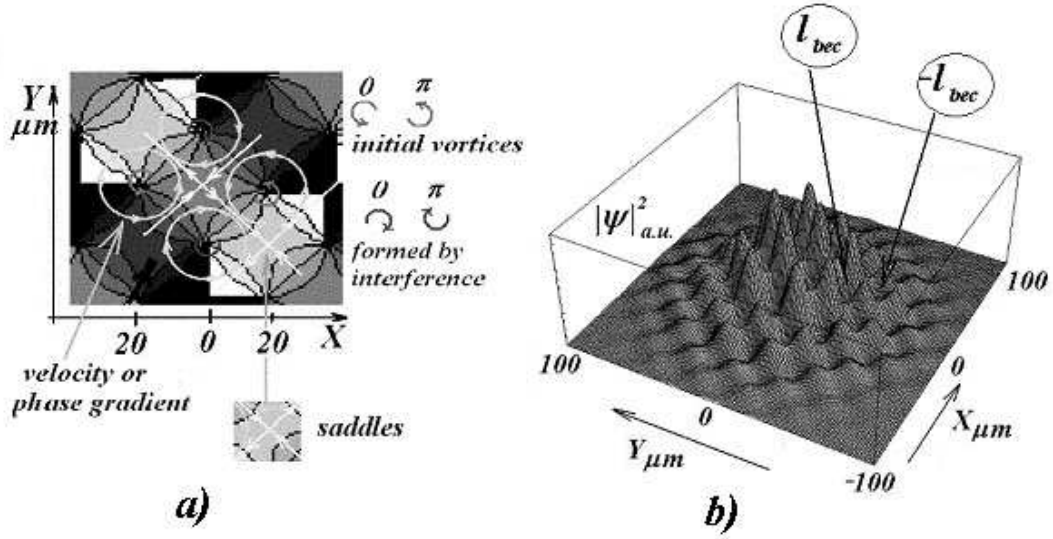


FIG. 5: a) The argument of macroscopic wavefunction Ψ and corresponding field of velocities obtained via Madelung transform. The superfluid vortices form the lattice with alternating topological charges $l_{BEC} = \pm 1$. The elementary cell consists of four BEC vortices whose locations are identical to the vortices of trapping EM-field. Horizontal pair has the same charges l_{BEC} which are π -shifted with respect to each other, the vertical pair have π -shifted $-l_{BEC}$ charges. The alternating charges l_{BEC} make the field of velocities continuous. b) The distribution of the square modulus of macroscopic wavefunction Ψ obtained via numerical modeling. The location of adjacent counter-rotating vortices l_{BEC} shown.